Highly efficient inverted polymer solar cell by low temperature annealing of Cs_2CO_3 interlayer

Hua-Hsien Liao,[2] Li-Min Chen,[1] Zheng Xu,[1] Gang Li,[3] and Yang Yang[1,a)]
[1]*Department of Materials Science and Engineering, University of California-Los Angeles, California 90095, USA*
[2]*Department of Electric Engineering, National Tsing Hua University, Hsinchu 300, Taiwan*
[3]*Solarmer Energy, Inc., El Monte, California 91731, USA*

(Received 18 January 2008; accepted 10 April 2008; published online 30 April 2008)

We demonstrate a highly efficient inverted bulk heterojunction polymer solar cell based on regioregular poly(3-hexylthiophene):[6,6]-phenyl C_{61} butyric acid methyl ester with a low temperature annealed interfacial buffer layer, cesium carbonate (Cs_2CO_3). This approach improves the power conversion efficiency of the inverted cell from 2.3% to 4.2%, with short-circuit current of 11.17 mA/cm^2, open-circuit voltage of 0.59 V, and fill factor of 63% under AM1.5G 100 mW/cm^2 irradiation. This result is comparable to the previous regular structure device on the same system. Ultraviolet photoelectron spectroscopy shows that the work function of annealed Cs_2CO_3 layer decreases from 3.45 to 3.06 eV. Further x-ray photoelectron spectroscopy results reveal that Cs_2CO_3 can decompose into low work function, doped cesium oxide Cs_2O upon annealing, which is accountable for the work-function reduction and device efficiency improvement. © *2008 American Institute of Physics*. [DOI: 10.1063/1.2918983]

Polymer photovoltaic (PV) cells have recently attracted a lot of attention due to their low-cost and easy-processing fabrication properties.[1,2] Polymer bulk heterojunction (BHJ) PV cell is the most promising structure, with a donor-acceptor blend sandwiched between the cathode and anode. The interpenetrated network of the donor-acceptor blend in the BHJ structure provides charge separation and charge transportation properties for achieving high efficiency. From device point of view, regioregular poly(3-hexylthiophene) (RR-P3HT) and highly soluble fullerene derivative [6,6]-phenyl C_{61} butyric acid methyl ester (PCBM) blend represents the state-of-the-art system.[3,4] By controlling the growth rate of RR-P3HT,[1] the improved polymer chain organizations enhance the hole mobility to the comparable level of electron, and the power conversion efficiency (PCE) of RR-P3HT:PCBM device can achieve 4.4%, with a regular device structure [indium tin oxide (ITO)/poly(3,4-ethylenedioxythiophene):poly(styrenesulfonate) (PEDOT:PSS)/RR-P3HT:PCBM/Ca/Al].[1,5,6] The regular structure consists of both an acidic PEDOT:PSS layer and a low work function metal cathode. The acidic PEDOT:PSS layer has been proven to be detrimental to the active polymer layer,[7–9] and the low work function metal cathode is easily oxidized by air even with a delicate encapsulation.[10,11] Both of them have a negative influence on the device lifetime. Recently, we addressed this issue by successful demonstration of an inverted polymer PV cell with 2.25% PCE by using cesium carbonate (Cs_2CO_3) to modify the polarity of ITO and highly transparent metal oxides, i.e., vanadium oxide (V_2O_5), as the anodic buffer layer.[12] Several inverted structures have also been proposed thereafter. White *et al.* utilized solution-processed ZnO on ITO and Ag as the transparent cathode and anode, respectively, and achieved 2.58% PCE.[13] Waldauf *et al.* adapted a solution-processed titanium oxide layer on ITO as the cathode and PEDOT:PSS as the anode to obtain 3% PCE.[14] Nevertheless, until nowadays, the PCEs of inverted polymer PV cells are still behind the regular ones.

In this letter, we demonstrate that the work function of Cs_2CO_3 can be modified from 3.45 to 3.06 eV by a low temperature (below 200 °C) annealing treatment, verified by ultraviolet photoelectron spectroscopy (UPS). With the inverted device structure (ITO/Cs_2CO_3/RR-P3HT:PCBM/V_2O_5/Al), the PCE improves from 2.31% to 4.19% by a 150 °C thermal annealing treatment of the Cs_2CO_3 interfacial layer. Generally, the decomposition temperature of Cs_2CO_3 is around 550–600 °C.[15] However, preliminary x-ray photoelectron spectroscopy (XPS) results reveal that thermal annealing process helps Cs_2CO_3 decompose into low work function cesium oxide although the temperature is much lower than previously reported.

The inset of Fig. 1(b) shows the inverted solar cell structure. 0.2 wt % Cs_2CO_3 dissolved in 2-ethoxyethanol was spin coated on precleaned and 15 min UV-ozone-treated ITO glass substrates as the cathode. Various annealing temperatures were carried out on the hot plate inside the glovebox for 20 min. RR-P3HT and PCBM were separately dissolved in 1,2-dichlorobenzene, then blended together with 1:1 wt/wt ratio to form a 2.5 wt % solution. This RR-P3HT/PCBM solution was spin coated at 600 rpm for 40 s, and the wet film was dried in a covered glass Petri dish. The dried film was then annealed at 110 °C for 10 min. The active film thickness was ~210–230 nm measured by a Dektak 3030 profilometer. The anode is 10 nm V_2O_5 covered by 100 nm Al. The devices were tested in the glovebox under simulated AM1.5G irradiation (100 mW/cm^2) by using a solar simulator. The illumination intensity was determined by a NREL calibrated Si detector with KG-5 color filter, and the spectral mismatch was corrected. VCA Optima™ contact angle measurement system (AST Products, Inc.) was used to determine the contact angle of water on the Cs_2CO_3 surfaces. XPS and UPS analyses were carried out in ultrahigh vacuum environment (Omicron Nanotechnology system). UPS spectra were

a)Electronic mail: yangy@ucla.edu.

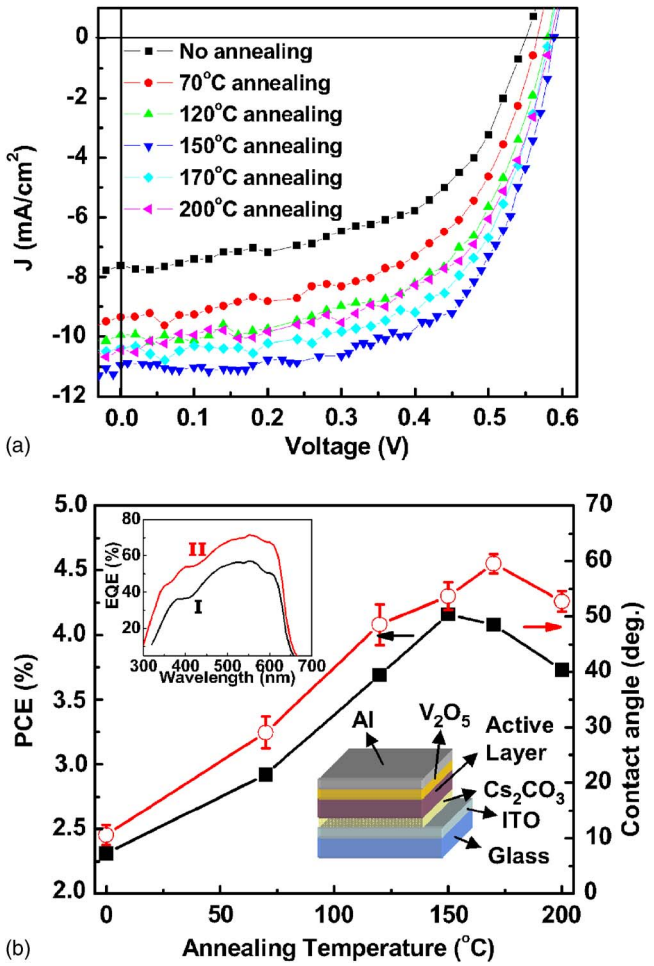

FIG. 1. (Color online) (a) *I-V* characteristics of the inverted PV devices under illumination with various annealing temperatures of the Cs_2CO_3 layer (b) Power conversion efficiency (PCE) and contact angle with water of the Cs_2CO_3 layer as a function of different annealing temperatures. The inset in (b) shows the effect of annealing treatment on external quantum efficiency. Line I is Cs_2CO_3 layer without annealing, and line II is after 150 °C annealing.

obtained by using He I line ($h\nu$=21.2 eV), and Al Kα radiation source ($h\nu$=1486.6 eV) was used for the XPS analysis.

Figure 1(a) shows *J-V* curves with different Cs_2CO_3 annealing temperatures. For the device without thermal annealing on Cs_2CO_3 layer, the PCE is 2.31%. When Cs_2CO_3 layers were treated by different temperature annealing process, all device performances improved. As the annealing temperature of Cs_2CO_3 layer increases from room temperature to 150 °C, the PCE increases from 2.31% to 4.19%. In addition, all other device characteristics, such as V_{OC}, I_{SC}, and fill-factor, improved as well. The device operation parameters are summarized in Table I. The optimum annealing temperature is determined within the range of 150–170 °C. In this annealing temperature range, the average device PCE is approximately 4%, and the highest PCE achieved is 4.2% for 150 °C annealing.

To understand the mechanism for this device performance improvement by thermal annealing process of the Cs_2CO_3 layer, contact angle measurement on Cs_2CO_3 surface is performed. A strong correlation between Cs_2CO_3 surface contact angle and device efficiency under different temperature treatments was observed, as shown in Fig. 1(b). The contact angle variation of water on Cs_2CO_3 surfaces follows the PCE results. Below 170 °C, the contact angle increases

TABLE I. Short-circuit current density (J_{sc}), open-circuit voltage (V_{oc}), power conversion efficiency (PCE), and fill factor (FF) of various inverted PV devices, and contact angle of Cs_2CO_3 layer with water upon different thermal annealing temperatures.

Anneal T (°C)	V_{oc} (V)	J_{sc} (mA/cm^2)	PCE (%)	FF (%)	Contact angle (θ)
N/A	0.550	7.61	2.31	55.2	11
70	0.565	9.36	2.92	55.2	29
120	0.580	10.86	3.69	58.6	49
150	0.590	11.13	4.19	64.0	54
170	0.582	11.29	4.08	62.1	60
200	0.584	11.39	3.73	56.0	53

with the Cs_2CO_3 layer annealing temperature, and decreases slightly above 170 °C. The increase of the contact angle indicates a surface property transition from hydrophilic to hydrophobic upon annealing of the Cs_2CO_3 layer, which is beneficial for polymer film growth. The surface contact angle reflects the surface energy, and the result clearly reveals that the thermal annealing of Cs_2CO_3 layer can modify the surface energy of the Cs_2CO_3 surface, which is speculated to be one of the reasons behind the enormously improved efficiency of inverted structure solar cell. Further Cs_2CO_3 surface property studies are carried out by UPS and XPS.

Figure 2 shows the secondary electron edge of Cs_2CO_3 films spin coated on ITO substrate, which provides the information of the work function modification by the Cs_2CO_3 layer and thermal annealing. The work function of UV-ozone-treated ITO substrate is 4.54 eV. When Cs_2CO_3 is spin coated on this ITO surface without thermal annealing, the work function changes to 3.23 eV. The work function of the Cs_2CO_3 film further reduces to 3.13, 3.11, and 3.06 eV after annealing at 70, 120, and 170 °C, for 20 min, respectively. For comparison, the work function of Cs_2CO_3 on Ag-coated Si substrates is also examined. The work function of Cs_2CO_3 on Ag also reduces from 3.45 (as cast) to 3.06 eV (annealing at 170 °C for 20 min, shown in the inset), which suggests that the decrease of the work function is mainly due

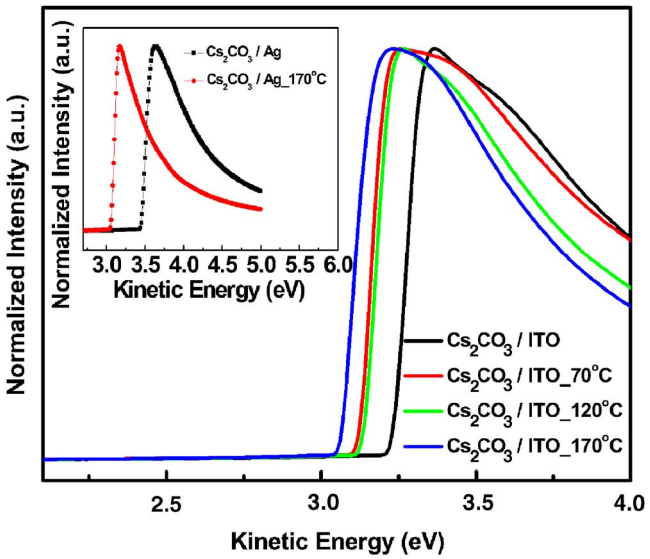

FIG. 2. (Color online) Evolution of secondary electron edge with various annealing temperatures of the Cs_2CO_3 layer. The inset shows the work-function reduction of the Cs_2CO_3 layer on Ag substrates due to the annealing treatment.

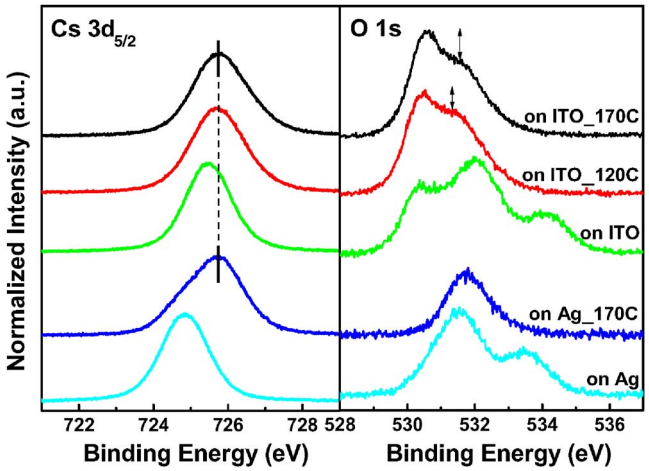

FIG. 3. (Color online) X-ray photoelectron spectroscopies of (a) Cs $3d_{5/2}$ and (b) O 1*s* with various annealing temperatures of the Cs_2CO_3 layer on ITO and Ag substrates.

to the intrinsic property of Cs_2CO_3 itself, rather than a chemical reaction between Cs_2CO_3 and the ITO substrate.

Figure 3 shows Cs $3d_{5/2}$ and O 1*s* spectra from XPS study of Cs_2CO_3 films. From the Cs $3d_{5/2}$ spectra in Fig. 3(a), Cs_2CO_3 film on ITO shows a higher binding energy than on Ag substrate, which can be attributed to the competitive bonding of In and Sn to oxygen with Cs, thus, decreasing the binding energy for Cs. Both Cs_2CO_3 spin coated on Ag or ITO substrates show that the Cs $3d_{5/2}$ shift toward higher binding energy upon annealing (a larger extent for Ag substrate) and have the same binding energy after annealing at 170 °C. This suggests that the decomposition of the cesium carbonate occurs for both substrates, also indicating that the decomposition is an intrinsic reaction.

For Cs_2CO_3 spin coated on ITO, from the O 1*s* spectra in Fig. 3(b), the O 1*s* spectra show three characteristic peaks, which are assigned to the ITO, cesium carbonate, and adsorbed oxygen peaks at 530.32, 532, and 534.16 eV, respectively. The adsorbed oxygen peak is seen for spin-coated Cs_2CO_3 films on both ITO and Ag substrates, and disappears upon subsequent annealing. Upon annealing, the adsorbed oxygen peak desorbs, and the relative ratio of the metal-oxide peak around 530.5 eV starts to increase, accompanied by decrease of the cesium carbonate peak, suggesting that the decomposition of Cs_2CO_3 into more oxidelike, which is consistent with the Cs $3d_{5/2}$ spectra result. For Cs_2CO_3 spin coated on Ag, the O 1*s* binding energy increases after annealing at 170 °C, which resembles band bending induced by *n*-type doping; this trend is also seen in all the other spectra.

The O:Cs ratio is calculated for Cs_2CO_3 spin coated and after annealing at 170 °C on Ag to exclude the oxygen contribution from the substrate. The O:Cs ratio varies from 1.8 to 0.84, implying that oxygen escapes from the Cs_2CO_3 film due to decomposition and produces cesium oxide. The O:Cs ratios are slightly higher than the stoichiometric values. This is due to residual solvent and oxygen adsorption during sample transfer before annealing; while after annealing, the sample is Cs_2O doped with Cs_2O_2, thus, a larger O:Cs ratio than the stoichiometic value. It has been previously reported that Cs_2CO_3 decomposes into stoichiometric Cs_2O doped with Cs_2O_2 during thermal evaporation,[15,16] and the current XPS results indicate that Cs_2CO_3, on both ITO or Ag substrates, decomposes to form an oxide Cs_2O and is possibly doped with Cs_2O_2. This doped cesium oxide behaves as a *n*-type semiconductor, with an lower interface resistance than pristine Cs_2CO_3, and a relatively low work function, which contributes to the improved performance upon annealing treatment.

To summarize, a highly efficient inverted polymer solar cell has been demonstrated by thermal annealing of Cs_2CO_3 layer. The achieved efficiency of 4.2% is comparable to our best result of the regular structure device. The UPS results show that the work function of the Cs_2CO_3 layer is decreased by thermal annealing, and preliminary XPS studies reveal that Cs_2CO_3 intrinsically decomposes into a doped *n*-type semiconductor by the annealing process. This highly efficient inverted cell can be applied to design a multiple-device stacked polymer solar cells or a tandem cell, which are widely accepted to further improve the efficiency of polymer solar cells.

The authors would like to acknowledge the financial support from Solarmer Inc., University of California Discovery Grant, and NSF IGERT: Materials Creation Training Program (MCTP) (DGE-0114443) and the California NanoSystems Institute. H.H.Liao would also like to thank the National Science Council of Taiwan, Project 096JFA04031 for financial support. The technical discussions with Dr. Jinsong Huang of Agiltron Inc. are also deeply appreciated.

[1] G. Li, V. Shrotriya, J. Huang, Y. Yao, T. Moriarty, K. Emery, and Y. Yang, Nat. Mater. **4**, 864 (2005).
[2] M. L. Ma, C. Y. Yang, X. Gong, K. Lee, and A. J. Heeger, Adv. Funct. Mater. **15**, 1617 (2005).
[3] L. H. Hoppe and N. S. Sariciftci, J. Mater. Chem. **16**, 45 (2006).
[4] G. Li, V. Shrotriya, Y. Yao, J. Huang, and Y. Yang, J. Mater. Chem. **17**, 3126 (2007).
[5] G. Li, Y. Yao, H. Yang, V. Shrotriya, G. Yang, and Y. Yang, Adv. Funct. Mater. **17**, 1636 (2007).
[6] C. Melzer, E. J. Koop, V. D. Mihailetchi, and P. W. M. Blom, Adv. Funct. Mater. **14**, 865 (2004).
[7] Y. Sahin, S. Alem, R. de Bettingnies, and J. M. Nunzi, Thin Solid Films **476**, 340 (2005).
[8] M. Y. Song, K. J. Kim, and D. Y. Kim, Sol. Energy Mater. Sol. Cells **85**, 31 (2005).
[9] A. Waranabe and A. Kasuya, Thin Solid Films **483**, 358 (2005).
[10] M. P. de Jong, L. J. van Ijzendoom, and M. J. A. de Voigt, Appl. Phys. Lett. **77**, 2255 (2000).
[11] G. Greczynski, Th. Kugler, M. Keil, W. Osikowicz, M. Fahlman, and W. R. Salaneck, J. Electron Spectrosc. Relat. Phenom. **121**, 1 (2001).
[12] G. Li, C. W. Chu, V. Shrotriya, J. Huang, and Y. Yang, Appl. Phys. Lett. **88**, 253503 (2006).
[13] M. S. White, D. C. Olson, S. E. Shaheen, N. Kopidakis, and D. S. Ginley, Appl. Phys. Lett. **89**, 143517 (2006).
[14] C. Waldauf, M. Morana, P. Denk, P. Schilinsky, K. Coakley, S. A. Choulis, and C. J. Brabec, Appl. Phys. Lett. **89**, 233517 (2006).
[15] A. H. Sommer, J. Appl. Phys. **51**, 1254 (1980).
[16] J. S. Huang, Z. Xu, and Y. Yang, Adv. Funct. Mater. **17**, 1966 (2007).